MOLEKUL
eISSN: 2503-0310

Articles
https://doi.org/10.20884/1.jm.2024.19.2.10295

Silver Nanoparticle Biosynthesis using *Distimake vitifolius* Extract for Enhancement of Antibacterial and Antioxidant Activity

Candra Yulius Tahya[1]*, Karnelasatri[2], Wahyu Irawati[3], Sri Wahyu Ningsih Munthe[2]

[1]Chemistry Education Study Program, Faculty of Education, Pelita Harapan University, Tangerang, Indonesia
[2]Pharmacy Study Program, Faculty of Health Sciences, Pelita Harapan University, Tangerang, Indonesia
[3]Biology Education Study Program, Faculty of Education, Pelita Harapan University, Tangerang, Indonesia

*Corresponding author email: candra.tahya@uph.edu

Received November 16, 2023; **Accepted** April 16, 2024; **Available online** July 20, 2024

ABSTRACT. The biological method for silver nanoparticle synthesis emphasizes green synthesis, which is faster, environmentally safer, facile, energy-efficient, and cost-effective. It provides good alternatives to physical and chemical methods. In this research, we have synthesized silver nanoparticles using *D. vitifolius* ethanolic extract. The 38 natural compounds of flavonoid, phenolic or polyphenol compositions have been determined by LC-MS/MS-QTOF which is carried out using UNIFI software equipped with a mass spectrum library of active substances from natural ingredients from the Waters database. Silver nanoparticle (Dv-AgNP) was characterized by using TEM and SEM where the average diameter of nanoparticle was seen <100 nm and confirmed by PSA analysis that the Z-average is 62.73 ± 0.71 nm. EDS spectrum confirmed the silver element as a major element of the particles. PI value of Dv-AgNP is 0.557, while the zeta potential is -17.37 ± 1.53 mV. Dv-AgNP can inhibit the growth of *P. aeruginosa* (amoxicillin resistant) with an inhibition zone of 15.83 ± 2.36 mm, and *K. pneumoniae* with an inhibition zone is 10.03 ± 0.55 mm. These are moderate inhibitory activities. The antioxidant result of the Dv-AgNP suspension solution shows that the IC_{50} is 0.58 mM. The IC_{50} of the crude extract is 752 ppm and is categorized as very weak antioxidant activity.

Keywords: Antibacterial; *D. vitifolius*; silver nanoparticle.

INTRODUCTION

Silver nanoparticles (AgNP) have attracted large interest of research works over the last few decades because it possesses variety of biological activities such as antibacterial, antiviral (Jeremiah et al., 2020), anticancer (Al-Sheddi et al., 2018), anti-inflammatory (Tyavambiza et al., 2021) and antifungal (Akintelu et al., 2021). In addition, it has been used in various applications i.e., drug delivery, biosensing, screening and medicines, cosmetics, gene engineering, tissue biotechnology, and so on (Singh et al., 2014; Skiba et al., 2020). The excellent antibacterial activity of AgNP has caught researchers' attention. AgNP with a larger surface-to-volume ratio (smaller particles) will have higher reactivity in hampering microbial growth. AgNP as an antibacterial agent has the potential to be used in the treatment of infectious and pathogenic bacterial diseases, especially with the alarming occurrence of multidrug resistance, causing death annually (Zhang et al., 2017). Silver nanoparticle-based devices are highly effective against both Gram-positive and Gram-negative bacteria and do not cause infections, they are frequently utilized in dental and cardiovascular implants (Almatroudi, 2020). This is related to the AgNP mechanism of action in various ways attacking various types of bacteria in multiple structures at one time (Bruna et al., 2021). The synthesis of AgNP with desirable shape and size can be conducted from physical, chemical, and biological methods. However, the physical, and chemical methods have the environmental concern due to the use of toxic chemicals and higher-cost production.

The biological method for AgNP synthesis emphasizes green synthesis, which is a faster, environmentally safer, facile, energy-efficient, and cost-effective method. It provides good alternatives to physical and chemical methods. Green synthesis involves all components of biological origin like natural extract, biopolymers, or microorganisms themselves that act as reducing agents, capping, and stabilizers for AgNP synthesis. AgNP green-mediated synthesis exhibits high solubility, yield, stability, and less toxic potential (Chung et al., 2016; Xi et al., 2016). Green synthesis AgNP could be carried out at milder conditions such as low temperatures, safer solvents, and less dangerous reagents to improve its biocompatibility, and adaptability in healthcare applications (Chung et al., 2016). AgNP synthesis from silver ion by biological extract may be triggered by several

functional groups such as carbonyl, amine, amide, and phenolic which are presented in terpenoids, alkaloids, flavonoids, polyphenols (Ritu et al., 2023), pigments, protein, polysaccharides, fatty acids, and other reductants intercellularly or extracellularly (Asmathunisha & Kathiresan, 2013). According to other reports, the silver nanoparticles produced by *C. nocturnum* extract were mostly spherical, had an average particle size of 20 nm, had more antioxidant activity than vitamin C, and strong antibacterial activity (highest against *Vibrio cholerae* and least against *E. faecalis*) (Keshari et al., 2020).

Plant extracts have enormous potential for the bioproduction of nanoparticles. The ability of plant extracts to produce nanoparticles has featured exciting loom towards the escalation of natural products. *Merremia vitifolia* is one of the plants in the Convolvulaceae family that is widely grown in Southeast Asian regions, including Indonesia. *M. vitifolia* currently named *Camonea vitifolia* and was reclassified to *Distimake vitifolius* (Pisuttimarn et al., 2023) is a well abundance around Tangerang regency, Indonesia. Several organic compounds have been identified based on Gas Chromatography-Mass Spectrometry (GC-MS) analysis with similarity index ≥ 89% which are caryophyllene, (E)-β-famesene, neophytadiene, phytol, 9,12,15-octadecatrienoic acid, 1,5-cyclodecadiene, squalene, stigmasterol, γ-sitosterol, Serratol, vitamin E and lup-20(29)-en-3-one (Tahya & Karnelasatri, 2021). Another report of LC-MS/MS analysis of n-hexane extract of *D. vitifolius* also identified chemicals such as spinasterol, stigmastan-3,6-dione, azedarachin C, trichosanic acid, stearidonic acid, and digiprolactone (Tahya et al., 2023). Many of those chemicals have the potency to be used as reducing agents for the formation of AgNP. *D. vitifolius* polar extract is a novel source of reducing agents to be used to synthesize silver nanoparticles (Dv-AgNP). This research is directed to examine how silver nanoparticles could be synthesized using ethanolic extract of *D. vitifolius*, then characterize the properties of Dv-AgNP using UV-Vis, FTIR, TEM, SEM, PSA, and evaluate the antibacterial and antioxidant properties of the Dv-AgNP.

EXPERIMENTAL SECTION

Plant Species Identification

A Fresh sample of leaves and twigs of the plant was collected, and a DNA extraction procedure was performed based on Zymo Research D4081 using Genomic DNA extraction with Quick-DNA Magbead Plus Kit. The PCR amplification was carried out with MyTaq HS Red Mix, 2X (Bioline, BIO-25048). PCR Master mix 1 x 25 µL is dd H_2O 9 µL, MyTaq Red Mix 2x 12.5 µL, 20 µM Rbcl-F Primer 1 µL, 20 µM Rbcl-R Primer 1 µL, and 20 µM Rbcl-R Primer 1 µL. Primer sequence Rbcl-F: ATGTCACCACCAACAGAG ACTAAAGC and Rbcl-R: GTAAAATCAAGTCCA CCRCG. Positive results of PCR were shown in gel electrophoresis. Then continue to Bi-directional DNA Sequencing using the BigDye® Terminator v3.1 cycle sequencing kit chemistry. DNA Sequence was submitted to NCBI Genbank.

Extraction of *D. vitifolius* Leaf

The dried powder of *D. vitifolius* leaf weighed as much as 110.65 g and 1000 mL of ethanol was mixed in the flask, shielded, and stirred for 2 x 6 hours, and left still for 2 days at room temperature. Then the mixture was filtered to get the ethanolic extract. All solvents were evaporated, and the crude extract was weighed. About 2.0 g of crude extract was taken for LC-MS/MS analysis and the Flavonoid-Phenolic content was analyzed.

LCMS/MS-QTOF Analysis of *D. vitifolius* Ethanolic Extract.

The sample preparation process is by weighing 1.0 g of sample into a 10 mL volumetric flask, then adding ethanol solvent then ultrasonic for 30 minutes and homogenizing. Filter with a 0.22 µm GHP/PTFE filter membrane then injected into the instrument. LC setup using column C1 with column temperature 40°C, autosampler temperature 15°C, and injection volume 10 µL. Mobile phase A 0.1% formic acid in acetonitrile and mobile phase B is 0.1% formic acid in distilled water. Flow rate 0.6 mL/min in gradient. MS settings mode of operation: ToF MSE ionization: ESI (-)/ ESI (+) acquisition range: 50-1200 Da. The screening process for active substances from natural ingredients using LCMS/MS-QTOF is carried out using UNIFI software which already has a mass spectrum library of active substances from natural ingredients from the Waters database. UNIFI software can identify the mass spectrum of compounds in the sample which is then matched with the mass spectrum in the library. Active substances are identified if they meet the requirements, including mass error in reading the analyte ≤ 5 ppm error. Isotope match MZ RMS PPM ≤ 6 ppm & Isotope match MZ RMS % ≤ 10 %. Analyte intensity ≥ 300 4.2.4. There is one fraction with a brake value < 4 in the Fragment match elucidation system.

Total Phenolic Content

Total phenolic was determined based spectroscopic method using Folin-Ciocalteu's reagent. The Total Phenolic Content was interpreted as gallic acid equivalent (mgGAE) per gram of the dried sample. Gallic acid was prepared in several serial concentrations (20, 40, 60, 80, and 100 ppm). 0.3 mL of each gallic acid solution mixed with 1.5 mL of 10% Folin-Ciocalteu's reagent and 1.2 mL of Na_2CO_3 7.5% and vortex and stored for 30 min in the dark at room temperature. The blank solution was also prepared. The absorbance was recorded using a spectrometer at 765 nm. The extract solution

of 1000 ppm was prepared and followed a similar process as gallic acid to determine the absorbance for the duplets experiment.

Total Flavonoid Content

The total flavonoid content of the *D. vitifolius* ethanolic extract was calculated by using the aluminium chloride method. 2 mL of sample was mixed with 2 mL of 2 % aluminium chloride and then vortexed. Serial concentrations of Quercetin were used to make the calibration curve. The extract was dissolved in ethanol to 1000 ppm. The absorbance of the mixtures was measured at 415 nm by using a spectrophotometer. The total flavonoid content was expressed in terms of quercetin equivalent (mg QE/g of sample). All the analyses were repeated two times.

Synthesis of Silver Nanoparticles

The crude extract was dissolved in ethanol in several variations of concentrations i.e., 1000 ppm, 500 ppm, and 250 ppm. Precisely, 20 ml of ethanolic extract solution was added to 100 ml silver nitrate solution (1 mM) in a 250 ml volumetric flask and stirred 6 hours every day for 4 days using a magnetic stirrer at room temperature. The change in color of the solution after 4 days indicated the reduction of silver nitrate into silver nanoparticles denoted as Dv-AgNP. Then 2 ml Dv-AgNP suspension solution was taken to measure the absorbance (λ 200-600 nm) using a UV-Vis spectrophotometer. The Dv-AgNP suspension solution was centrifuged at 10000 rpm for 15 min and the pellet was collected. Further, the pellets were dried in an oven at 70°C for 3 h. The Dv-AgNP powder and characterized by Scanning Electron Microscopy (SEM-EDS) and Fourier Transform Infra-Red spectroscopy (FTIR). Then Transmission Electron Microscopy (TEM) analysis and Particle Size Analyzer (PSA) were used to analyze the suspension solution of Dv-AgNP for measurement of the morphology, particle size, and zeta potential.

Antioxidant Activity 2,2-Diphenyl-1-Picrylhydrazyl (DPPH) Method

The free radical scavenging activity of crude extract, Dv-AgNP, and standard vitamin C was determined using the stable radical DPPH. IC_{50} value of crude extract was determined using the variation of crude extract concentrations of 1000, 800, 600, 400, and 200 ppm. For antioxidant IC_{50} value of vitamin C was determined using variations of concentration of 20, 15, 10, and 5 ppm. For the antioxidant IC_{50} value of the nanoparticle, the suspension solution was used. The suspension solutions of Dv-AgNP were diluted in several concentrations. Exact 1 mL of each sample solution was mixed with 1.5 mL of DPPH solution and absorbance was read in 517 nm. The formula for inhibitory percentage is as follows:

$$\% \text{ Inhibitory} = \frac{blank\ absorbance - sample\ absorbance}{blank\ absorbance} \times 100\%$$

Antibacterial Activity of Dv-AgNP

Antibacterial activity was tested by the disc diffusion method. A total of 6 grams of Luria Broth Agar (LBA) was dissolved with distilled water in 150 mL and then sterilized by autoclave at 121°C for 15 minutes. About 20 mL LBA liquid was poured into sterile petri dishes and let for several minutes until solidified. Then the LBA media was inoculated with 20 μL of *Pseudomonas aeruginosa* and *Klebsiella pneumoniae* suspension. The paper disc was dripped with 20 μL of various samples including crude extract solution 25000 ppm, suspension Dv-AgNP solution, and amoxicillin 1000 ppm. Commercial amoxicillin product in tablet form was used to make amoxicillin 1000 ppm. Then, it was incubated in an incubator at 30°C for 24 hours. The antibacterial assay was carried out by measuring the Diameter of Inhibition Area around the disc paper, then the results were classified based on CLSI (Clinical and Laboratory Standards Institute) provisions.

RESULTS AND DISCUSSION

Plant Species Identification

One effective taxonomic approach for identifying and discovering new species is DNA barcoding. One or more standardized short DNA sections are used in DNA barcoding to identify taxa. DNA barcoding techniques are used to find the universal barcode gene, such as COI in metazoans, rbcL, matK, and ITS in plants, ITS in fungus, and 16S rRNA gene in bacteria and archaea (Antil et al., 2023). In this report, we identify plant based on rbcL gene. PCR product electrophoresis is shown in **Figure 1a**. Based on the DNA sequencing of the plant shows high similarity to the *M. vitifolia* ribulose-1,5-bisphosphate carboxylase/oxygenase large subunit (rbcL) gene (**Figure 1b**).

We observe an intense band of DNA in agarose gel around 650 bp di PCR product (**Figure 1a**), and the rbcL gene has been sequenced. The DNA sequence of rbcL gene (642 bp) of *D. vitifolius* was submitted to GenBank with accession number **OR689565**. The BLAST results show that this plant gene has the highest similarity to *M. vitifolia* (100%), and strong similarity to other species such as *M. dissecta* (99.82%), *M. quinguefolia* (99.65%), *D. dissectus* (99.82%), *Cressa cretica* (99.47%) and *Tephrosia nubica* (99.47%) (**Figure 1b**). As previously mentioned, *M. vitifolia* has been reclassified as *D. vitifolius* (Pisuttimarn et al., 2023). This analysis confirms the previous morphology identification in the previous report (Tahya et al., 2023). Based on the phylogenetic analysis of BLAST (**Figure 1c**), the sample gene denoted as 'merremia sp' (yellow highlighted) has 100% similarity to *M. vitifolia* ribulose-1,5-bisphosphate carboxylase/oxygenase large subunit (rbcL) gene.

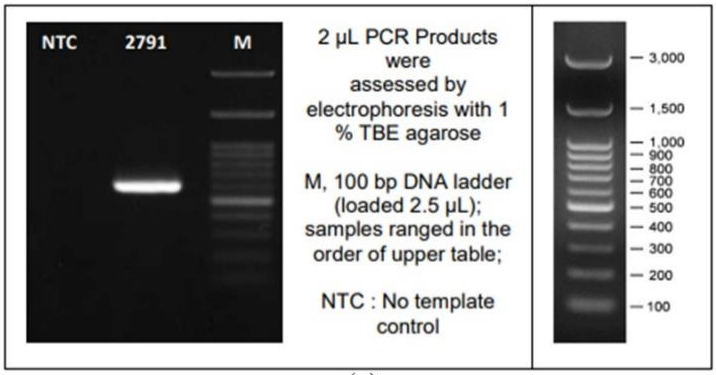

(a)

Description	Max Score	Total Score	Query Cover	E value	Per. Ident	Accession
Merremia vitifolia ribulose-1,5-bisphosphate carboxylase/oxygenase large subunit (rbcL) gene, partial cds; chloroplast gene for chloroplast...	1053	1053	99%	0.0	100.00%	AY100981.1
Merremia dissecta ribulose-1,5-bisphosphate carboxylase/oxygenase large subunit (rbcL) gene, complete cds; chloroplast gene for chloro...	1048	1048	99%	0.0	99.82%	AY100979.1
Merremia quinquefolia chloroplast, partial genome	1042	1042	99%	0.0	99.65%	KF242501.1
Distimake dissectus voucher Trotta950015 ribulose-1,5-bisphosphate carboxylase/oxygenase large subunit (rbcL) gene, partial cds; chlor...	1040	1040	99%	0.0	99.82%	MH549825.1
Cressa cretica isolate UQU ALP178 ribulose-1,5-bisphosphate carboxylase/oxygenase large subunit (rbcL) gene, partial cds; chloroplast	1037	1037	99%	0.0	99.47%	MH598910.1
Tephrosia nubica isolate UQU ALP150 ribulose-1,5-bisphosphate carboxylase/oxygenase large subunit (rbcL) gene, partial cds; chloroplast	1037	1037	99%	0.0	99.47%	MH598893.1
Operculina turpethum Chaw 1581 chloroplast DNA, complete genome	1037	1037	99%	0.0	99.47%	LC729560.1
Ipomoea biflora Chaw 1599 chloroplast DNA, complete genome	1037	1037	99%	0.0	99.47%	LC729550.1
Ipomoea biflora voucher FJ05992020122102 plastid, complete genome	1037	1037	99%	0.0	99.47%	NC_060786.1
Operculina macrocarpa chloroplast, partial genome	1037	1037	99%	0.0	99.47%	KF242502.1

(b)

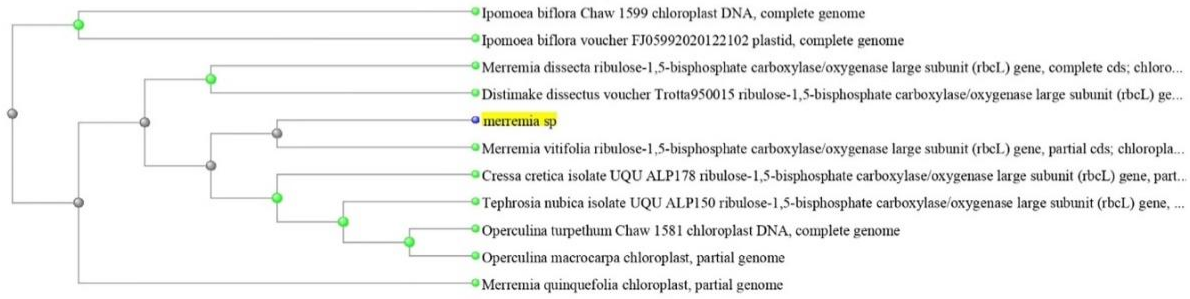

(c)

Figure 1. (**a**) PCR product electrophoresis with 1 % TBE agarose and marker 100 bp DNA Ladder. (**b**) The top 10 hit BLAST results against the NCBI database, excluding uncultured sample sequences. (**c**) Phylogenetic analysis of BLAST data. Based on the data we can determine the taxonomy of this plant: Equisetopsida → Solanales → Convolvulaceae → Distimake → *D. vitifolius* (Burm.f.) Pisuttimarn & Petrongari, 2023, homotypic synonym: *M. vitifolia* (Burm.f.) Hallier f., 1893.

Total Phenolic and Flavonoid Content of the Extract

Natural extracts high in phenolic and flavonoid compounds that have antioxidant properties have sparked attention in recent decades. Natural flavonoids and phenolic substances are secondary metabolites found in plants that have at least one hydroxyl group attached to an aromatic ring. Since phenolic compounds' hydroxyl groups can directly support antioxidant activity, they make good electron donors (Aryal et al., 2019). Moreover, a few of them promote the cell's natural production of antioxidant molecules. Peroxide decomposition, oxygen scavenging, metal inactivation, and free radical inhibition are all demonstrated by phenolic compounds in biological systems, and they also reduce the burden of oxidative illness (Côté et al., 2010). In this report, the dry weight of crude extract obtained is 3.7203 g (3.36%) from 110.65 g of leaf powder. The total phenolic and flavonoid content is shown in **Table 1**. Based on the data, we can see that the total phenolic and flavonoid content of *D. vitifolious* are categorized as low and intermediate, respectively. As comparison the phenolic contents varied among the species; *A. sessilis*, *C. tora*, and *P. oleracea* had the high phenolic content (292.65 ± 0.42, 287.73 ± 0.16, and 216.96 ± 0.87 mg GAE/g, respectively), while *B. alba*, *I. aquatica*, and *S. nigrum* had the low phenolic content (72.66 ± 0.46, 77.06 ± 0.70, and 97.96 ± 0.62 mg GAE/g, respectively) (Aryal et al., 2019). Meanwhile, *I. aquatica*, *B. alba*, and *S. nigrum* had the low quantities of flavonoids (6.61 ± 0.42, 6.97 ± 0.62, and 16.42 ± 0.39 mg QE/g, respectively), whereas *P. oleracea*, *C. tora*, and *L. cephalotes* had the high flavonoid content (39.38 ±

0.57, 37.86 ± 0.53, and 36.95 ± 0.44 mg QE/g, respectively) (Aryal et al., 2019).

Identification of Flavonoid and Phenolic Compounds by LC-MS/MS-QTOF

The ethanolic extract of *D. vitifolius* was analyzed by LC-MS/MS-QTOF (**Figures 2** and **3**). Several flavonoids, polyphenols, and phenolic compounds have been identified as listed in **Tables 2 and 3**. Plant extract containing a variety of compounds was reported to initiate the biosynthesis of silver nanoparticles, including flavonoids, phenolics, alkaloids, terpenoids, flavones, amines, amides, and pigments. Flavonoids and terpenoids are most likely responsible for the stabilization of the AgNP (Asmathunisha & Kathiresan, 2013). Another study states that the bioreduction and precipitation of AgNP are facilitated by a variety of secondary metabolites found in plants, including flavonoids, terpenoids, ketones, carboxylic acid, amides, proteins, and enzymes. These metabolites also act as capping and stabilizing agents (Khanal et al., 2022).

Table 1. TPC and TFC results data

Analysis	Concentration	Regression equation
Total Phenolic Content (TPC)	30.47 ± 1.88 mg GA/g of extract	$y = 0.0101x + 0.0232$ $R^2 = 0.9985$
Total Flavonoid Content (TFC)	19.42 ± 0.16 mg QE/g of extract	$y = 0.0359x + 0.0274$ $R^2 = 0.9989$

Note: values are mean ± SD (n = 3)

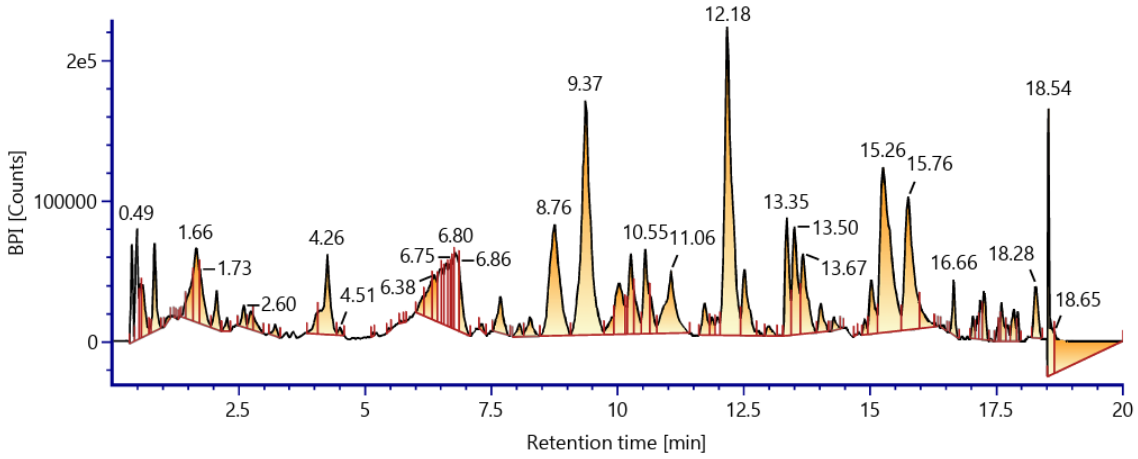

Figure 2. Chromatogram of LC-MS/MS-QTOF ESI (+) mode of *D. vitifolius* crude extract.

Table 2. List of Flavonoid and Phenolic compounds in ethanolic extract identified by LC-MS/MS-QTOF using ESI (+) Mode.

No	ESI Mode	Component name	Formula	Observed RT (Min)	Mass error (ppm)	Isotope Match Mz RMS PPM	Isotope Match Intensity RMS Percent	Response	Adducts
				FLAVONOID					
1	(+)	2-Hydroxy-4-methyl acetophenone	$C_9H_{10}O_2$	2.49	-4.4	4.19	8.40	20498	+H
2	(+)	6-Methoxykaempferol-3-O-β-D galactopyraniside	$C_{22}H_{22}O_{12}$	10.57	-1.9	2.31	3.30	120817	+H
3	(+)	Kaempferol-3-glucuronide	$C_{21}H_{20}O_{12}$	9.39	-0.9	1.14	2.01	186990	+H
4	(+)	Maltol	$C_6H_6O_3$	3.43	-4.6	4.76	7.90	14454	+H
5	(+)	Quercetin-3-O-glucuronide 6"-methyl ester	$C_{22}H_{20}O_{13}$	10.72	-2.3	2.79	6.01	42765	+H

6	(+)	Quercetin-3-O-α-D-glucuronide	$C_{21}H_{18}O_{13}$	9.32	-0.7	1.08	3.84	199516	+H
				PHENOLIC					
1	(+)	2-Ethyl-4, 5-dimethyl-phenol	$C_{10}H_{14}O$	8.74	-5.9	5.71	4.52	5285	+H
2	(+)	3,5-O-Dicaffeoylquinic acid	$C_{25}H_{24}O_{12}$	9.99	-2.3	2.55	7.47	56321	+H
3	(+)	Dihydroeugenol	$C_{10}H_{14}O_2$	14.69	-3.9	3.69	4.98	3450	+H
4	(+)	Moupinamide	$C_{18}H_{19}NO_4$	12.19	-0.9	1.16	4.67	543832	+H
5	(+)	N-trans-Coumaroyltaramine	$C_{17}H_{17}NO_3$	11.73	-1.9	2.23	6.49	83888	+H
6	(+)	Tribulusamide A	$C_{36}H_{36}N_2O_8$	14.03	-1.4	1.66	6.27	141058	+H

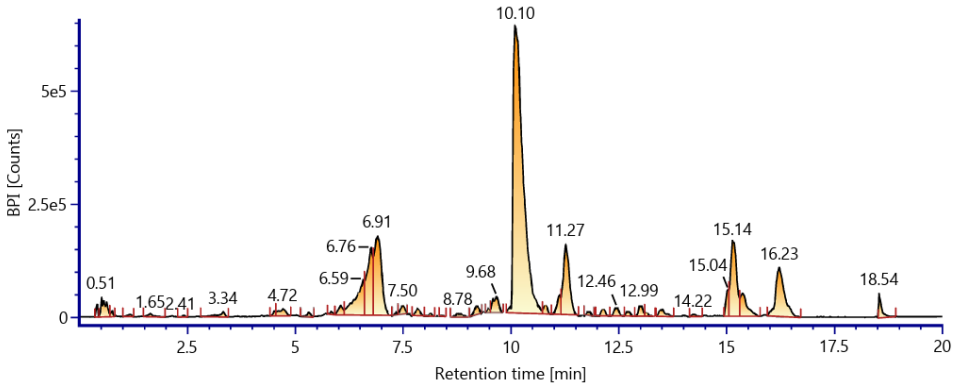

Figure 3. Chromatogram of LC-MS/MS-QTOF ESI (-) mode of *D. vitifolius* crude extract.

Table 3. List of Flavonoid and Phenolic compounds in ethanolic extract identified by LC-MS/MS-QTOF using ESI (-) Mode.

No	ESI Mode	Component name	Formula	Observed RT (Min)	Mass error (ppm)	Isotope Match Mz RMS PPM	Isotope Match Intensity RMS Percent	Response	Adducts
				FLAVONOID					
1	(-)	(+)-Catechin-pentaacetate	$C_{25}H_{24}O_{11}$	11.75	-1.3	1.51	2.20	10110	-H
2	(-)	5,7-Dimethoxy-4'-hydroxy flavone-4'-O-α-L-rhamnose(12)-β-D-glucoside	$C_{29}H_{34}O_{14}$	12.06	-0.9	1.22	7.83	25913	-H
3	(-)	5-Hydroxy-7-methoxy flavanone	$C_{16}H_{14}O_4$	16.59	-1.2	2.92	8.24	899	-H
4		6-Methoxykaempferel-3-O-β–D-galactopyranoside	$C_{22}H_{22}O_{12}$	10.80	-2.5	0.28	2.13	116488	-H
5	(-)	Chrysoeriol-4' -O-β-D-glucopyranoside	$C_{22}H_{22}O_{11}$	11.59	-1.5	1.75	1.67	14705	-H
6	(-)	Cnidimol C	$C_{10}H_8O_5$	7.29	-3.3	1.97	9.45	781	-H

7	(-)	Epicatechin gallate (Epicatechin-3-O-gallate)	$C_{22}H_{18}O_{10}$	15.50	-1.5	1.60	8.14	414	-H
8	(-)	Epigallocatechin-3-O-gallate	$C_{22}H_{18}O_{11}$	14.37	0.5	2.73	6.73	454	-H
9	(-)	Homoeriodictyol	$C_{16}H_{14}O_6$	15.02	-2.2	2.27	5.92	1071	-H
10	(-)	Odoratin-7-O-β-D-glucoside	$C_{22}H_{24}O_9$	12.14	-3.1	0.54	2.06	72754	-H
11	(-)	Prunetin-4′-glucoside	$C_{22}H_{22}O_{10}$	12.48	-2.1	0.89	5.85	12329	-H
12	(-)	Quercetin-3-gentiobioside	$C_{27}H_{30}O_{17}$	8.07	1.5	3.44	3.17	8902	-H
13	(-)	Quercetin-3-O-glucuronide 6"-methyl ester	$C_{22}H_{20}O_{13}$	10.96	-1.7	0.66	2.98	17165	-H
14	(-)	Quercetin-3-O-α-D-glucuronide	$C_{21}H_{18}O_{13}$	9.61	-2.3	0.34	3.35	178206	-H
15	(-)	Rhamnetin	$C_{16}H_{12}O_7$	15.73	-2.2	1.86	6.00	3560	-H
			POLYPHENOL						
1	(-)	1,3,5-O-Tricaffeoyl-quinic acid	$C_{34}H_{30}O_{15}$	13.92	0.4	2.09	2.59	12427	-H
			PHENOLIC						
1	(-)	2,4, 5-Trihydeoxybenzaldehyde	$C_7H_6O_4$	6.16	-3.8	4.03	8.15	7024	-H
2	(-)	2,4,6-Trihydroxyacetophenone-2,4-di-O-β-D-glucopyranoside	$C_{20}H_{28}O_{14}$	6.70	-1.5	1.00	2.28	17693	-H
3	(-)	3,4-Dihydroxybenzamide	$C_7H_7NO_3$	13.61	-4.0	3.54	0.87	19739	-H
4	(-)	3,5-O-Dicaffeoylquinic acid	$C_{25}H_{24}O_{12}$	10.55	-2.6	0.50	7.98	244229	-H
5	(-)	4,5-O-Dicaffeoylquinic acid	$C_{25}H_{24}O_{12}$	11.13	-2.3	0.38	3.75	206302	-H
6	(-)	4-Hydroxyacetophenone	$C_8H_8O_2$	6.30	-2.7	5.52	7.10	13028	-H
7	(-)	Aspidinol	$C_{12}H_{16}O_4$	14.74	-3.0	1.89	2.48	1037	-H
8	(-)	Cimidahurine	$C_{14}H_{20}O_8$	5.75	-2.2	1.54	7.14	42107	-H
9	(-)	Ethyl caffeate	$C_{11}H_{12}O_4$	13.17	-3.6	1.70	2.79	15959	-H
10	(-)	Homoarbutin	$C_{13}H_{18}O_7$	4.97	-0.8	2.92	5.11	804	-H
11	(-)	Methyl-B-orsellinate	$C_9H_{10}O_4$	10.41	-2.0	4.44	3.21	893	-H
12	(-)	Protocatechuic aldehyde	$C_7H_6O_3$	4.71	-3.6	4.50	4.13	60822	-H
13	(-)	Tribulusamide A	$C_{36}H_{36}N_2O_8$	14.24	-0.5	1.55	4.44	33669	-H
14	(-)	1 -O-Methyl-3,5-O-dicaffeoylquinic acid methyl ester	$C_{27}H_{28}O_{12}$	13.32	-0.5	1.95	5.28	9853	-H

Based on the LC-MS/MS ESI (+) mode, 12 flavonoid and phenolic compounds have been identified. With the ESI (-) mode, there are 15 flavonoid dan 15 phenolic (including 1 polyphenolic) compounds that have been identified. In **Table 2** (ESI (+)), Quercetin-3-O-α-D-glucuronide is the most abundant compound. A report shows that α-glucosidase activity was inhibited by quercetin-3-O-glucuronide (Q3GA), with an IC_{50} value of 108.11 ± 4.61 µM (Xing, Chun, Qiang, Xiong, & Rui-Hai, 2021). Other report said that quercetin 3-O-β-D-Glucuronide has anti-inflammatory, antioxidant, moisturizing, and antimelanogenesis effects in human keratinocytes and melanoma cells via NF-κB and AP-1 activation (Ha et al., 2022). Meanwhile, in **Table 3** (ESI (-)), compounds named 3,5-O-Dicaffeoylquinic acid (DEQA) are found to be most abundant. According to a study, the administration of DEQA therapy reduced the formation of type I procollagen and inhibited the UVA-mediated rise in MMP-1 production. These results raise the possibility that DEQA may one day be used as a cosmetic agent to cure and prevent skin photoaging (Oh et al., 2020).

Characterization of Silver Nanoparticle

The UV-Vis spectrum of Dv-AgNP is shown in **Figure 4**. The extract has a green-yellowish color, and it did not show any change in color after 4 days of stirring, while the silver nanoparticle solution changed from green-yellowish to yellow-redish and finally to brown. The color changer of the silver nanoparticle solution was an indication of the reduction of Ag^+ to Ag^0 that took place in the solution at a temperature of around 27°C. The Extract has a maximum absorbance of 416 nm, while the maximum absorbance of Dv-AgNP is 384 nm.

The color of the Dv-AgNP is brown. The maximum absorbance of Dv-AgNP is different from several reports that the maximum absorbance is 416-450 nm (Khanal et al., 2022; Singh et al., 2018). Meanwhile, Uddin et al., (2020) reported the maximum absorbance of silver nanoparticles that were synthesized using *Cocos nucifera* leaf extract is 380 nm (Uddin et al., 2020). Elamawi et al., (2018) report biosynthesis of silver nanoparticles using *Trichoderma longibrachiatum* has a maximum absorbance of 385 nm (Elamawi et al., 2018) which is quite similar to this report and also another report in 393 nm (Hegazy & Borham, 2018). The AgNP has an absorption band based on the surface plasmon resonance spectrum with a lot of free electrons because the combined electron's vibration of AgNP is in resonance with a light wave.

The functional groups of crude extract and the Dv-AgNP were determined using FTIR. The result of FTIR analysis is shown in **Figure 5(a)** and **Table 4**.

The functional groups implicated in the capping and stabilizing actions were verified by comparing the positions of the peaks in the FTIR spectra of the extract and the AgNP. **Table 4** displays the recorded IR spectra of the extract and AgNP for various functional groups within the 500–4000 cm^{-1} range (**Figure 5a**). A large peak in the extract's spectra at 3396.2 cm^{-1} is displaced to 3424 cm^{-1} in the AgNP. It results from the plant's polyphenols' hydrogen-bonded -OH group expanding frequently. The C-O stretching of ether linkages seen in flavones that are adsorbed on the surface of the biogenic material is reflected in the shifting of vibrations at 1075 to 1050 cm^{-1}. The extract's peak at 2852.8 cm^{-1} shifts to a higher wavenumber in the AgNP at 2853.8 cm^{-1}, which is associated with the stretching of alkanes' or aldehydes' sp^3-hybridized C-H. The FTIR peaks at 1732.2 cm^{-1} and 1630.2 cm^{-1} indicate the existence of aromatic C=C bonds, as well as C=O and C=C bonds. The stretching of an aromatic amine's carbon-nitrogen bond is correlated with the position of the peaks at 13782.3 cm^{-1} in AgNP.

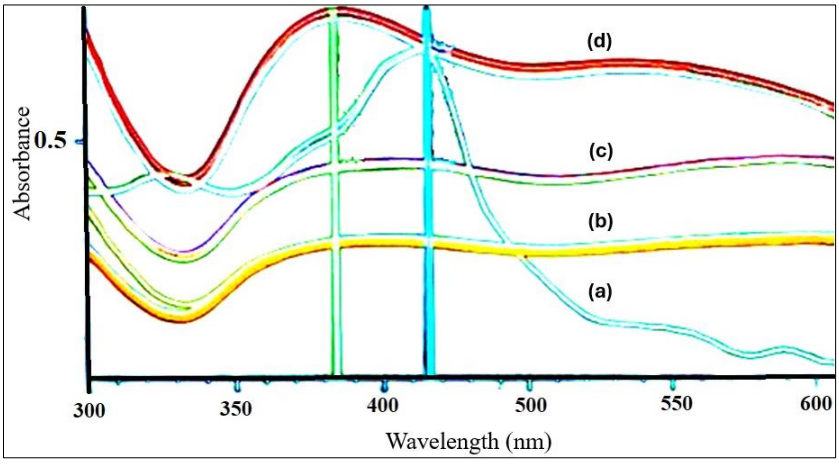

Figure 4. UV-vis spectrum of crude extract and Dv-AgNP solutions. (a) Solution of 1000 ppm extract in ethanol. (b) solution of Dv-AgNP as a product of 250 ppm extract solution + 1 mM $AgNO_3$. (c) solution of Dv-AgNP as a product of 500 ppm extract solution + 1 mM $AgNO_3$. (d) solution of Dv-AgNP as a product of 1000 ppm extract solution + 1 mM $AgNO_3$.

Table 4. The FTIR spectrum interpretation to the functional groups.

Dv-AgNP		*D. vitifolius* Crude Extract	
Wavenumber (cm^{-1})	Peak Assignment(s)	Wavenumber (cm^{-1})	Peak Assignment(s)
805.4	Amine (primary, aliphatic) N-H Stretch Benz.1,3-disub Aromatic C-H Bending Benz.1,4-disub Benz.1,2,4-trisub Benz.1,3,5-trisub	718.8	Amine (primary, aromatic) Aromatic C-H Bending Benz.1,3-disub Benz.1,2,3-trisub
1050.2	Alcohol/Phenol O-H & C-O Stretch Esters unconjugated C=O & C-O Stretch	1075	Alcohol/Phenol O-H & C-O Stretch Esters unconjugated C=O & C-O Stretch
1254	CH_3-X (X=halogen)	1260.6	CH_3-X (X=halogen) CH_3-Si(R1,R2,R3)
1378.3	R-C-CH_3-R CH_3-C(=O)-O	1378.6	R-C-CH_3-R CH_3-C(=O)-O
1456.3	Aromatic C=C Bend. & Strech CH_3-O-R CH_3-NR-C(=O)- amides	1400.6	Ammonium ion CH_3-N=(R1,R2) Aromatic C=C Bend. & Strech
1630.2	Alkenyl C-H & C=C Stretch Amide N-H & C=O Stretch	1636.5	Alkenyl C-H & C=C Stretch Amide N-H & C=O Stretch
1732.2	Aldehydes C=O unconjugated Stretch also C-H stretch 2700 & 2900	1738.6	Aldehydes C=O unconjugated Stretch also C-H stretch 2700 & 2900 Esters unconjugated C=O & C-O Stretch
2853.8	Alkyl C-H Stretch Carboxylic Acid C=O & O-H Stretch unconjugated Methylene (-CH_2-) C-H stretch	2852.8	Alkyl C-H Stretch Methylene (-CH_2-) C-H stretch
2922.7	Ammonium ion	2924.5	Ammonium ion
3424	Alcohol/Phenol O-H & C-O Stretch Amine (primary, aliphatic) N-H Stretch	3396.2	Alcohol/Phenol O-H & C-O Stretch Amine (primary, aliphatic) N-H Stretch

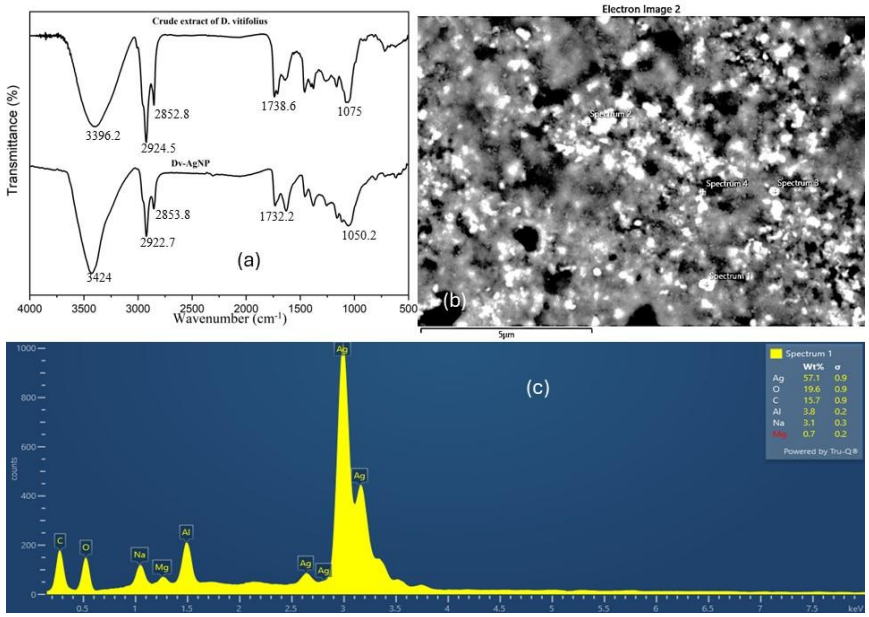

Figure 5. (a) FTIR Spectrum of Dv_AgNP compared to crude extract, (b) SEM image of Dv-AgNP in 20000x magnification, and (c) EDS spectrum of Dv-AgNP.

Table 5. Particle size and zeta potential analysis results.

Parameters	Measurement			Mean	SD
	1	2	3		
Z-Average (nm)	62.1	62.6	63.5	62.73333	0.71
Polydispersity Index (PI)	0.553	0.563	0.555	0.557	0.0053
Zeta Potential Mean (mV)	-15.7	-18.7	-17.7	-17.3667	1.53
Electrophoretic Mobility Mean (Cm^2/Vs)	-0.00012	-0.00015	-0.00014	-0.00013	0.000012

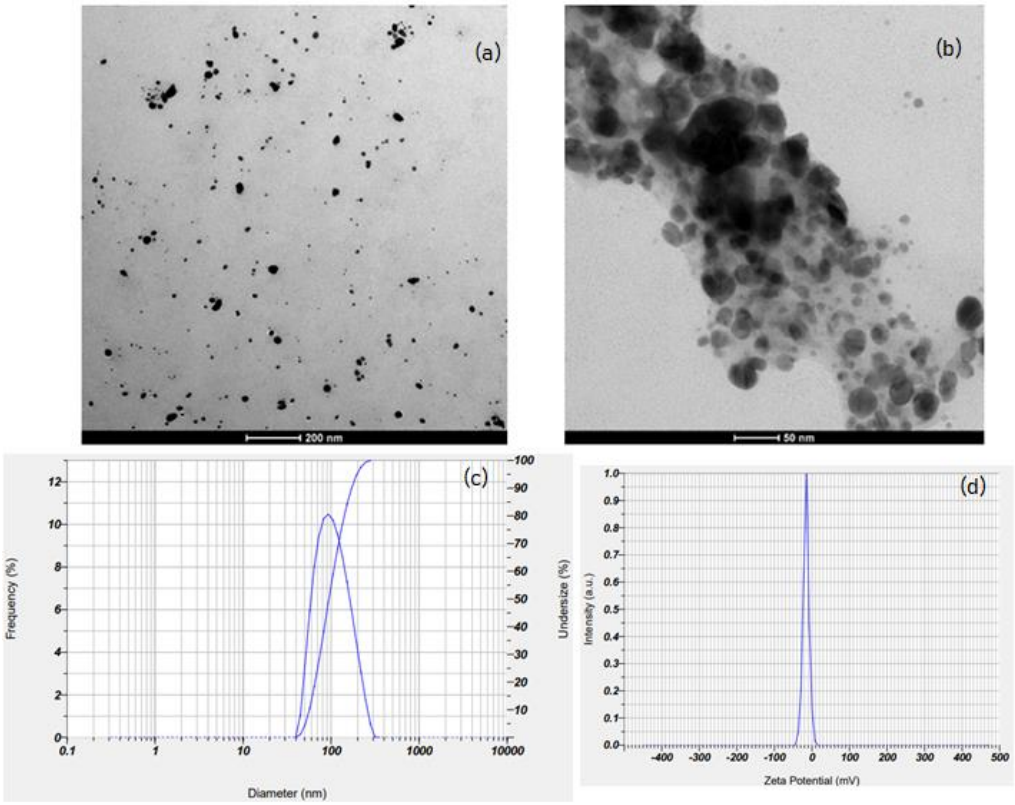

Figure 6. (a) TEM Image of Dv-AgNP in 29000x magnification, (b) TEM Image Dv-AgNP in 145000x magnification. (c) Particle size analysis of Dv-AgNP and (d) Zeta potential of Dv-AgNP.

Scanning Electron Microscopy shows that the size of the particle is way smaller than 5 µm, and based on the EDS spectrum the main element in the Dv-AgNP is silver (57.1 wt%). Oxygen is 19.6%, carbon is 15.7%, while other elements, aluminum (Al), sodium (Na), and magnesium (Mg) also exist in the particle. The particle size of Dv-AgNP can be confirmed using Particle Size Analyzer (PSA) as shown in **Figure 6(c)** and **Table 5**. This PSA test was carried out using the Dynamic Light Scattering (DLS) method using the Horiba-Sz 100z PSA. The sample was mounted with cuvette cells. A polydispersity index (PI) (<0.7) can occur because the sample is well-soluted/dispersed. The colloidal stability and the value of the polydispersity index are connected. The solution visual precipitation may occur if the dispersions' polydispersity index value is equal to or greater than 1. A value of less than 0.3 for the polydispersity index indicates better colloidal characteristics (Haque et al., 2017). Dv-AgNP has good colloidal characteristics because the PI value ranges from 0.553-0.563. The z-Average of Dv-AgNP is 62.73 ± 0.71 nm. The particle of Dv-AgNP is a nanoparticle because the average size is less than 100 nm. The Zeta Potential depends on the surface charge, which reflects the stability of silver nanoparticles in suspension and is also an important factor in the initial adsorption of AgNP into the cell membrane thus influencing its toxicity against bacteria (Rasmussen, Pedersen, & Marie, 2020). The zeta potential of Dv-AgNP range from -18.7 to -15.7 mV or at average -17.37 ± 1.53 mV (**Table 5**) with a single peak in **Figure 6(d)**, signifying the presence of repulsion among the synthesized silver nanoparticles (Elamawi et al., 2018) and a characteristic of stable silver nanoparticle (Ismail et al., 2021).

TEM Image of Dv-AgNP supports PSA and SEM Image, as we see in **Figure 6**(**a**) dan **6**(**b**), the size of the particle is less than 100 nm, the shape of the particle is spherical and there are capping structures around silver nanoparticles. This is confirming that *D. vitifolious* extract can act as a reducing agent in the

biosynthesis of silver nanoparticles. A report showed that AgNP (97.04 nm in diameter size) was synthesized by *Muntingi calabura* leaf extract (Wahab et al., 2018). Even, smaller average particle size was reported less than 50 nm for silver nanoparticles synthesized by *P. eldarica* bark extract (Iravani & Zolfaghari, 2013). This finding just reconfirms that the biological methods in nanoparticle synthesis appear to be simple, fast, and can produce well-defined size and morphology under optimized conditions for research. As reducing agents, bacterial protein or plant extracts allow us to regulate the nanoparticles' size, shape, and monodispersity (Gurunathan et al., 2009; Islam et al., 2021).

Antibacterial Activity Test

Antibacterial tests were performed against two pathogenic bacteria, *K. pneumoniae* and *P. aeruginosa.* These bacteria were isolated and identified in previous research (Irawati et al., 2022; Irawati et al., 2023). The antibacterial test result can be seen in **Table 6** and **Figure 7**. Dv-AgNP suspension solution as a product of 1000 ppm extract solution + 1 mM $AgNO_3$ was used in this test. Based on the Clinical and Laboratory Standard Institute, the Dv-AgNP shows inhibitory activity against the growth of *P. aeruginosa* (15.83 ± 2.36 mm) (moderate activity) and *K. pneumoniae* (10.03 ± 0.55 mm) (low activity) in **Figure 7** as also confirmed by others (Ezealisiji et al., 2017; Khanal et al., 2022). Nevertheless, crude extract of *D. vitifolius* 25000 ppm and the solvent of Dv-AgNP, did not inhibit the growth of both bacteria. Another study also reports that several plant extracts do not inhibit the growth of several bacteria (Keshari et al., 2020). The antibiotic amoxicillin 1000 ppm cannot inhibit the growth of *P. aeruginosa* because of the resistance over amoxicillin (Varela et al., 2021). Several reports have shown that *P. aeruginosa* is resistant to several antibiotics including amoxicillin (Hussain et al., 2017). Antibiotics such as penicillin, ampicillin, cefixime, and cefpodoxime were reported to be resisted by *P. aeruginosa* (Mapipa et al., 2021). *K. pneumoniae* growth can be inhibited by both Dv-AgNP suspension solution and amoxicillin 1000 ppm. The inhibition zone of AgNP was confirmed by another report to be higher than the antibacterial activity of $AgNO_3$ (Keshari et al., 2020). Although it has been thoroughly investigated, AgNP's precise antibacterial mechanism has not yet been verified. The antibacterial activity of AgNP is explained by numerous theories. By generating reactive oxygen species (ROS) and entangling themselves in the bacteria's cell, then the silver nanoparticles kill the bacteria (Urnukhsaikhan et al., 2021). Furthermore, it is proposed that the AgNPs adhere to the bacteria, engage with their cell walls, and ultimately destroy them by blocking their membrane permeability(Dakal et al., 2016; Ezealisiji et al., 2017). It is also explained that AgNPs interact with enzymes and amino acids to produce reactive oxygen species, which either destroy the cells or impair their ability to operate. The nucleus's soft bases, such as phosphorus and sulfur, are interacting with silver nanoparticles, damaging DNA and ultimately leading to cell death (Ezealisiji et al., 2017).

Table 6. Diameter of inhibition zone against *K. pneumoniae* and *P. aeruginosa*.

Bacteria	Inhibition zone diameter (mm)				
	Extract solution 25000 ppm	Dv-AgNP suspension solution	Solvent (17% Ethanol)	DMSO	Amoxicillin 1000 ppm
	(1)	(2)	(3)	(4)	(5)
Klebsiella pneumoniae	0	10.03 ± 0.55	0	0	10.93 ± 0.81
Pseudomonas aeruginosa	0	15.83 ± 2.36	0	0	0

Note: values are mean ± SD (n = 3)

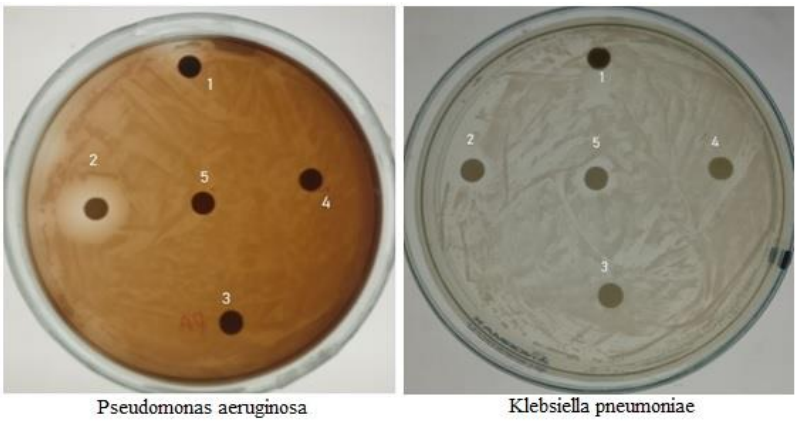

Figure 7. Disc diffusion antibacterial test of Dv-AgNP against *P. aeruginosa* and *K. pneumoniae*. (1) 25000 ppm extract solution, (2) Dv-AgNP suspension solution, (3) ethanol 17% (solvent), (4) DMSO, and (5) amoxicillin 1000 ppm.

Table 7. Antioxidant result of vitamin C

Vit. C (ppm)	Inhibition (%) y = -81.566x + 100 R^2 = 1	IC_{50}
0	0	
5	11.82	
10	38.66	12.27 ppm
15	64.68	
20	84.50	

Note: values are mean (n = 3)

Table 8. Antioxidant result of *D. vitifolius* extract.

Concentration of extract (ppm)	Inhibition (%) y = -0.0008x + 1.2286 R^2 = 0.9962	IC_{50}
0	0	
200	15.55 ± 0.72	
400	29.24 ± 2.68	752 ppm
600	41.39 ± 1.61	
800	53.46 ± 0.66	
1000	64.35 ± 1.61	

Note: values are mean ± SD (n = 3)

Table 9. Antioxidant result of Dv-AgNP suspension solution.

Suspension solution of Dv-AgNP	Ethanol volume	Inhibition (%) y = 87.698x - 0.5028 R^2 = 0.9886	the supposed concentration of the Dv-AgNP solution	IC_{50}
0 mL	100 mL	0	0	
20 mL	80 mL	18.042	0.2 mM	
40 mL	60 mL	31.056	0.4 mM	0.58 mM
60 mL	40 mL	54.127	0.6 mM	

Note: values are mean (n = 3). Suspension Dv-AgNP used is the solution of Dv-AgNP as a product of 1000 ppm extract solution 100 mL + 1 mM $AgNO_3$ 20 mL. Supposedly, [$AgNO_3$] = [Dv-AgNP].

Antioxidant Activity Test

The antioxidant activity test using DPPH methods was performed and the results are shown in **Table 7 – 9**. The antioxidant activity of vitamin C is categorized as strong (IC_{50} is 12.27 ppm), while the crude Ethanolic extract solution have very weak antioxidant activity. The ethanolic extract has IC_{50} 752 ppm. As a comparison, the aqueous extract of *D. vitifolius* has an antioxidant activity IC_{50} value is 146.61 µg/mL (Akter et al., 2021) higher than the ethanolic extract of *D. vitifolius*. Dv-AgNP suspension solution showed IC_{50} value at a concentration of 0.58 mM with the assumption that [$AgNO_3$] = [Dv-AgNP].

The idea was put forth to suggest that the adsorption of bioactive chemicals from leaf extract over spherically structured nanoparticles is responsible for the enhanced antioxidant capabilities of nanoparticles over extract (Küp et al., 2020). The scientists claim that the presence of phenolic chemicals, terpenoids, and flavonoids in plants is what gives AgNPs their antioxidant capacity and enables the nanoparticles to function as hydrogen donors, reducing agents, and singlet oxygen quenchers (Elemike et al., 2017).

CONCLUSIONS

The silver nanoparticle has been biosynthesized using ethanolic extract of *D. vitifolius*. The characterization of silver nanoparticles (Dv-AgNP) has been conducted using TEM and SEM where the diameter of the particle was seen <100 nm and confirmed by PSA analysis that the Z-average is 62.73 ± 0.71 nm. EDS spectrum confirmed the silver element as a major element of the particles. PI value of Dv-AgNP is 0.557, while the zeta potential is -17.37 ± 1.53 mV. Dv-AgNP can inhibit the growth of *P. aeruginosa* (amoxicillin-resistant) and *K. pneumoniae* with moderate activity. The antioxidant result of the Dv-

AgNP suspension solution shows that the IC_{50} is 0.58 mM. The IC_{50} of the crude extract is 752 ppm and is categorized as very weak antioxidant activity.

ACKNOWLEDGEMENTS

Thanks to The Centre of Research and Community Service (CRCS) UPH which is providing research funds with contract number P-106-FIP/I/2023.

REFERENCES

Akintelu, S. A., Olugbeko, S. C., & Folorunso, A. S. (2021). Green synthesis, characterization, and antifungal activity of synthesized silver nanoparticles (AgNPS) from *Garcinia kola* pulp extract. *BioNanoScience, 12,* 105–115. https://doi.org/10.1007/s12668-021-00925-3

Akter, S., Jahan, I., Khatun, R., Khan, M. F., Arshad, L., Jakaria, M., & Areeful Haque, M. (2021). Pharmacological insights into *Merremia vitifolia* (Burm.f.) Hallier f. leaf for its antioxidant, thrombolytic, anti-arthritic and anti-nociceptive potential. *Bioscience Reports*, *41*(1), BSR20203022. https://doi.org/10.1042/BSR20203022

Almatroudi, A. (2020). Silver nanoparticles: Synthesis, characterisation and biomedical applications. *Open Life Sciences*, *15*(1), 819–839. https://doi.org/10.1515/biol-2020-0094

Al-Sheddi, E. S., Farshori, N. N., Al-Oqail, M. M., Al-Massarani, S. M., Saquib, Q., Wahab, R., … Siddiqui, M. A. (2018). Anticancer potential of green synthesized silver nanoparticles using extract of *Nepeta deflersiana* against human cervical cancer cells (HeLA). *Bioinorganic Chemistry and Applications*, *2018,* 9390784. https://doi.org/10.1155/2018/9390784

Antil, S., Abraham, J. S., Sripoorna, S., Maurya, S., Dagar, J., Makhija, S., … Toteja, R. (2023). DNA barcoding, an effective tool for species identification: a review. *Molecular Biology Reports*, *50*(1), 761–775. https://doi.org/10.1007/s11033-022-08015-7

Aryal, S., Baniya, M. K., Danekhu, K., Kunwar, P., Gurung, R., & Koirala, N. (2019). Total phenolic content, flavonoid content and antioxidant potential of wild vegetables from western Nepal. *Plants*, *8*(4), 96. https://doi.org/10.3390/plants8040096

Asmathunisha, N., & Kathiresan, K. (2013). A review on biosynthesis of nanoparticles by marine organisms. *Colloids and Surfaces B: Biointerfaces*, *103*, 2013, 283–287. https://doi.org/10.1016/j.colsurfb.2012.10.030

Bruna, T., Maldonado-Bravo, F., Jara, P., & Caro, N. (2021). Silver nanoparticles and their antibacterial applications. *International Journal of Molecular Sciences*, *22*(13), 7202. https://doi.org/10.3390/ijms22137202

Chung, I. M., Park, I., Seung-Hyun, K., Thiruvengadam, M., & Rajakumar, G. (2016). Plant-mediated synthesis of silver nanoparticles: Their characteristic properties and therapeutic applications. *Nanoscale Research Letters*, *11*(1), 40. https://doi.org/10.1186/s11671-016-1257-4

Côté, J., Caillet, S., Doyon, G., Sylvain, J.-F., & Lacroix, M. (2010). Bioactive compounds in cranberries and their biological properties. *Critical Reviews in Food Science and Nutrition*, *50*(7), 666–679. https://doi.org/10.1080/10408390903044107

Dakal, T. C., Kumar, A., Majumdar, R. S., & Yadav, V. (2016). Mechanistic basis of antimicrobial actions of silver nanoparticles. *Frontiers in Microbiology*, *7*, 1831. https://doi.org/10.3389/fmicb.2016.01831

Elamawi, R. M., Al-Harbi, R. E., & Hendi, A. A. (2018). Biosynthesis and characterization of silver nanoparticles using *Trichoderma longibrachiatum* and their effect on phytopathogenic fungi. *Egyptian Journal of Biological Pest Control*, *28*, 28. https://doi.org/10.1186/s41938-018-0028-1

Elemike, E. E., Fayemi, O. E., Ekennia, A. C., Onwudiwe, D. C., & Ebenso, E. E. (2017). Silver nanoparticles mediated by Costus afer leaf extract: Synthesis, antibacterial, antioxidant and electrochemical properties. *Molecules : A Journal of Synthetic Chemistry and Natural Product Chemistry*, *22*(5), 701. https://doi.org/10.3390/MOLECULES22050701

Ezealisiji, K. M., Noundou, X. S., & Ukwueze, S. E. (2017). Green synthesis and characterization of monodispersed silver nanoparticles using root bark aqueous extract of *Annona muricata* linn and their antimicrobial activity. *Applied Nanoscience (Switzerland)*, *7*(8), 905–911. https://doi.org/10.1007/s13204-017-0632-5

Gurunathan, S., Kalishwaralal, K., Vaidyanathan, R., Venkataraman, D., Pandian, S. R. K., Muniyandi, J., Hariharan, N., Eom, S.H. (2009). Biosynthesis, purification and characterization of silver nanoparticles using *Escherichia coli*. *Colloids and Surfaces B: Biointerfaces*, *74*(1), 328–335. https://doi.org/10.1016/J.COLSURFB.2009.07.048

Ha, A. T., Rahmawati, L., You, L., Hossain, M. A., Kim, J. H., & Cho, J. Y. (2022). Anti-inflammatory, antioxidant, moisturizing, and antimelanogenesis effects of quercetin 3-o-β-d-glucuronide in human keratinocytes and melanoma cells via activation of nf-κb and ap-1 pathways. *International Journal of Molecular Sciences*, *23*(1), 433. https://doi.org/10.3390/ijms23010433

Haque, M. N., Kwon, S., & Cho, D. (2017). Formation and stability study of silver nano-particles in

aqueous and organic medium. *Korean Journal of Chemical Engineering*, *34*(7), 2072–2078. https://doi.org/10.1007/s11814-017-0096-z

Hegazy, M. A., & Borham, E. (2018). Preparation and characterization of silver nanoparticles homogenous thin films. *NRIAG Journal of Astronomy and Geophysics*, *7*(1), 27–30. https://doi.org/10.1016/j.nrjag.2018.04.002

Hussain, M. S., Nasir, B., Shahid, H., Sarwar, F., & Ejaz, A. (2017). Prevalence and antibiogram of *Pseudomonas aeruginosa* isolated from clinical samples in a tertiary care hospital. *Journal of Medical and Scientific Research*, *8*(2), 1185–1188. https://doi.org/10.17727/jmsr.2018/6-8

Iravani, S., & Zolfaghari, B. (2013). Green synthesis of silver nanoparticles using *Pinus eldarica* bark extract. *BioMed Research International*, *2013*, 639725. https://doi.org/10.1155/2013/

Irawati, W., Tahya, C. Y., & Greisnaningsi. (2022). *Pantoea agglomerans, Klebsiella pneumoniae*, and *Shigella flexneri* isolated from the cisadane river as multiresistant bacteria to copper and dyes. *Indonesian Journal of Biotechnology*, *27*(4), 176–186. https://doi.org/10.22146/ijbiotech.66103

Irawati, W., Yuwono, T., Pinontoan, R., & Lindarto, V. (2023). Optimising wastewater treatment: Acinetobacter sp. IrC1 as a potential multi-resistant bacterium for copper accumulation and dyes decolourisation. *Tropical Life Sciences Research*, *34*(3), 37–56. https://doi.org/10.21315/ tlsr2023.34.3.3

Islam, M. A., Jacob, M. V., & Antunes, E. (2021). A critical review on silver nanoparticles: From synthesis and applications to its mitigation through low-cost adsorption by biochar. *Journal of Environmental Management*, *281*, 111918. https://doi.org/10.1016/J.JENVMAN.2020.111918

Ismail, G. A., El-Sheekh, M. M., Samy, R. M., & Gheda, S. F. (2021). Antimicrobial, antioxidant, and antiviral activities of biosynthesized silver nanoparticles by phycobiliprotein crude extract of the *Cyanobacteria spirulina* platensis and Nostoc linckia. *BioNanoScience*, *11*(2), 355–370. https://doi.org/10.1007/s12668-021-00828-3

Jeremiah, S. S., Miyakawa, K., Morita, T., & Yamaoka, Y. (2020). Potent antiviral effect of silver nanoparticles on SARS-CoV-2. *Biochemical and Biophysical Research Communications*, *533*(1), 195–200. https://doi.org/10.1016/j.bbrc.2020.09.018

Keshari, A. K., Srivastava, R., Singh, P., Yadav, V. B., & Nath, G. (2020). Antioxidant and antibacterial activity of silver nanoparticles synthesized by *Cestrum nocturnum*. *Journal of Ayurveda and Integrative Medicine*, *11*(1), 37–44. https://doi.org/10.1016/j.jaim.2017.11.003

Khanal, L. N., Sharma, K. R., Paudyal, H., Parajuli, K., Dahal, B., Ganga, G. C., Kalauni, S. K. (2022). Green synthesis of silver nanoparticles from root extracts of *Rubus ellipticus* sm. and comparison of antioxidant and antibacterial activity. *Journal of Nanomaterials*, *2022*, 1832587. https://doi.org/10.1155/2022/1832587

Küp, F. Ö., Çoşkunçay, S., & Duman, F. (2020). Biosynthesis of silver nanoparticles using leaf extract of *Aesculus hippocastanum* (horse chestnut): Evaluation of their antibacterial, antioxidant and drug release system activities. *Materials Science and Engineering C*, *107*, 110207. https://doi.org/10.1016/j.msec.2019.110207

Mapipa, Q., Digban, T. O., Nnolim, N. E., & Nwodo, U. U. (2021). Antibiogram profile and virulence signatures of *Pseudomonas aeruginosa* isolates recovered from selected agrestic hospital effluents. *Scientific Reports*, *11*(1), 11800. https://doi.org/10.1038/s41598-021-91280-6

Oh, J. H., Karadeniz, F., Kong, C. S., & Seo, Y. (2020). Antiphotoaging effect of 3,5-dicaffeoyl-epi-quinic acid against uva-induced skin damage by protecting human dermal fibroblasts in vitro. *International Journal of Molecular Sciences*, *21*(20), 7756. https://doi.org/10.3390/ijms21207756

Pisuttimarn, P., Simões, A. R. G., Petrongari, F. S., Simão-Bianchini, R., Barbosa, J. C. J., de Man, I., … Chatrou, L. W. (2023). Distimake vitifolius (convolvulaceae): reclassification of a widespread species in view of phylogenetics and convergent pollen evolution. *Botanical Journal of the Linnean Society*, *202*(3), 363–388. https://doi.org/10.1093/botlinnean/boac077

Rasmussen, M. K., Pedersen, J. N., & Marie, R. (2020). Size and surface charge characterization of nanoparticles with a salt gradient. *Nature Communications*, *11*(1), 2337. https://doi.org/10.1038/s41467-020-15889-3

Ritu, Verma, K. K., Das, A., & Chandra, P. (2023). Phytochemical-based synthesis of silver nanoparticle: Mechanism and potential applications. *BioNanoScience*, *13*(3), 1359–1380. https://doi.org/10.1007/s12668-023-01125-x

Singh, H., Du, J., Singh, P., & Yi, T. H. (2018). Ecofriendly synthesis of silver and gold nanoparticles by *Euphrasia officinalis* leaf extract and its biomedical applications. *Artificial Cells, Nanomedicine and Biotechnology*, *46*(6), 1163–1170. https://doi.org/10.1080/21691401.2017.1362417

Singh, R., Sahu, S. K., & Thangaraj, M. (2014). Biosynthesis of silver nanoparticles by marine invertebrate (polychaete) and assessment of its efficacy against human pathogens. *Journal of Nanoparticles*, *2014*, 718240. https://doi.org/10.1155/2014/718240

Skiba, M. I., Vorobyova, V. I., Pivovarov, A., & Makarshenko, N. P. (2020). Green synthesis of silver nanoparticles in the presence of polysaccharide: Optimization and characterization. *Journal of Nanomaterials*, *2020*, 3051308. https://doi.org/10.1155/2020/ 3051308

Tahya, C. Y., Karnelasatri, & Gaspersz, N. (2023). Chemical profiling and histamine inhibitory activity assessment of *Merremia vitifolia* and Bidens pilosa extracts. *Molekul*, *18*(1), 117–130. https://doi.org/10.20884/1.JM.2023.18.1.6833

Tahya, C. Y., & Karnelasatri, K. (2021). Gas chromatography-mass spectrometry analysis and α-glucosidase inhibitory activity of n-hexane extract of bilajang bulu (merremia vitifolia) leaves. *Walisongo Journal of Chemistry*, *4*(2), 162–172. https://doi.org/10.21580/wjc.v4i2.9427

Tyavambiza, C., Elbagory, A. M., Madiehe, A. M., Meyer, M., & Meyer, S. (2021). The antimicrobial and anti-inflammatory effects of silver nanoparticles synthesised from *Cotyledon orbiculata* aqueous extract. *Nanomaterials*, *11*(5), 1343. https://doi.org/10.3390/nano11051343

Uddin, A. K. M. R., Siddique, Md. A. B., Rahman, F., Ullah, A. K. M. A., & Khan, R. (2020). *Cocos nucifera* leaf extract mediated green synthesis of silver nanoparticles for enhanced antibacterial activity. *Journal of Inorganic and Organometallic Polymers and Materials*, *30*(9), 3305–3316. https://doi.org/10.1007/s10904-020-01506-9

Urnukhsaikhan, E., Bold, B.-E., Gunbileg, A., Sukhbaatar, N., & Mishig-Ochir, T. (2021). Antibacterial activity and characteristics of silver nanoparticles biosynthesized from Carduus crispus. *Scientific Reports*, *11*(1), 21047. https://doi.org/10.1038/s41598-021-00520-2

Varela, M. F., Stephen, J., Lekshmi, M., Ojha, M., Wenzel, N., Sanford, L. M., … Kumar, S. H. (2021). Bacterial resistance to antimicrobial agents. *Antibiotics*, *10*(5), 593. https://doi.org/10.3390/antibiotics10050593

Wahab, A. W., Karim, A., La Nafie, N., Nurafni, N., & Sutapa, I. W. (2018). Synthesis of silver nanoparticles using *Muntingia calabura* L. leaf extract as bioreductor and applied as glucose nanosensor. *Oriental Journal of Chemistry*, *34*(6), 3088–3094. https://doi.org/10.13005/ojc/340652

Xi, F. Z., Zhi, G. L., Wei, S., & Gurunathan, S. (2016). Silver nanoparticles: synthesis, characterization, properties, applications, and therapeutic approaches. *International Journal of Molecular Sciences, 17(9),* 1534. https://doi.org/10.3390/ijms17091534

Xing, X., Chun, C., Qiang, H., Xiong, F., & Rui-Hai, L. (2021). Investigation into the mechanisms of quercetin-3-O-glucuronide inhibiting α-glucosidase activity and non-enzymatic glycation by spectroscopy and molecular docking. *Food & Function*, *12*(17), 7825–7835. https://doi.org/10.1039/D1FO01042E

Zhang, W., Zhao, X. J., Jiang, Y., & Zhou, Z. (2017). *Citrus pectin* derived silver nanoparticles and their antibacterial activity. *Inorganic and Nano-Metal Chemistry*, *47*(1), 15–20. https://doi.org/10.1080/15533174.2015.1137073